KSCE Journal of Civil Engineering (2013) 17(6):1251-1262
DOI 10.1007/s12205-013-0074-x

Geotechnical Engineering
www.springer.com/12205

Numerical Modelling Study of the Load Sharing Law of Anti-sliding Piles based on the Soil Arching Effect for Erliban Landslide, China

Changdong Li*, Huiming Tang, Xinli Hu***, and Liangqing Wang******

Received March, 15 2011/Revised March, 8 2012/Accepted May 14, 2012

Abstract

This paper presents a new model of the load sharing law with a three-stage load sharing pattern via a representative case study in the Three Gorges reservoir region, China. A definitive new three-stage load transfer pattern is presented, including end-bearing soil arching, friction soil arching and the sliding mass in front of the pile. By means of the soil arching effect between the anti-sliding pile and landslide mass, the law of the load sharing ratio under different cases, including different intervals, section dimensions, driving forces, and shearing parameters of the sliding mass and the pile-soil interface, is presented by using the explicit finite-difference numerical modelling method. The results show that (a) the effect scale of the soil arching effect is within the scale of four times of the width of the pile; (b) the soil arching only exits within a certain pile interval, and it will become inefficiency beyond the maximum pile interval; (c) there is a threshold value for the cohesion strength parameters of the sliding mass, beyond which the load sharing ratios of soil arching keep in a steady level.

Keywords: *landslide, anti-sliding pile, load sharing ratio, soil arching effect, numerical modelling*

1. Introduction

With the rapid development of worldwide economic construction, many people are severely threatened or potentially threatened by landslides. To control this kind of geological hazard, the anti-sliding pile has been developed, and it is now considered one of the most significant measures for controlling landslides (Won *et al.*, 2005). Wang and Sassa (2003) examined the characteristics and movement of landslides and debris flows. Jiang and Yamagami (2006, 2008) presented a new method to determine the strength parameters from slips in homogeneous slopes. Wang and Sassa (2002, 2010) proposed landslide simulations by a geotechnical model combined with a model for apparent friction change. Using the scale effect law, Li *et al*. (2010) presented a new model for slope stability evaluation.

The importance of landslide control has inspired many studies, which have tackled the problem from various points of view, including theory analysis and test studies.

With respect to the theoretical research on pile-soil interaction, many researchers are now realizing the importance of the soil arching effect in explaining the pile-soil interaction. Ito and Matsui (1975) presented the limit lateral pressure calculation formula by the movement of the soil mass according to the plastic deformation theory. Shen (1992) stated that a complete anti-sliding limit design method should include all kinds of computations to check for failure, and he has offered several such computations through granular media limit theory. Wei *et al*. (2009) examined the slope reinforced with one row of piles using strength reduction analysis.

Initial research on the soil arching effect was presented by Terzaghi (1943) with his famous trap-door test in 1943. Several decades later, Vardoulakis *et al*. (1981) proposed a new concept of the "transition state" of the soil arching effect. Furthermore, Chevalier *et al*. (2007) proved the existence of a "transition state" of the effect in detail and introduced the deliberate trap-door test, which is the latest significant test for the soil arching effect.

Tests studies, including laboratory and numerical modelling tests, on landslides have been widely accepted all over the world. In early stages, many scholars have studied pile-soil interaction by laboratory modelling tests. Franx and Boonstra (1948), Heyman (1965), Leussink and Wenz (1969), De Beer and Wallays (1972), Poulos (1973) and Wenz (1973) have carried out site tests of piles under the horizontal movement of soil mass. Ito

*Senior Lecturer, Dept. of Geotechnical and Engineering Geology Faculty of Engineering, China University of Geosciences (Wuhan), Wuhan 430074, China (E-mail: lichangdong@ cug.edu.cn)
**Professor, Vice President, China University of Geosciences (Wuhan), Wuhan 430074, P.R. China (Corresponding Author, E-mail: tanghm@cug.edu.cn; hmtang6205@sina.com)
***Professor, Faculty of Engineering, China University of Geosciences (Wuhan), Wuhan 430074, P.R. China (E-mail: huxinli@cug.edu.cn)
****Professor, Faculty of Engineering, China University of Geosciences (Wuhan), Wuhan 430074, P.R. China (E-mail: wlq027@126.com)

and Matusi (1975) analysed the influence of pile design on the internal force distribution. Matsui *et al*. (1982) developed a method to detect the relationship between the soil pressure on the anti-sliding pile and the displacement of soil mass by using an iron box with different types of soil and anti-sliding pile.

With the fast development of numerical modelling technology, many scholars have focused their attention on the pile-soil interaction by conducting numerical modelling tests. For instance, Jeong *et al*. (2003) and Won *et al*. (2005) presented the soil-pile coupling analysis by simulation modelling software. Martin and Chen (2005), Fan and Long (2005) and Uzuoka *et al*. (2007) discussed the response to the anti-sliding pile under the condition of slope horizontal movement with different kinds of numerical simulation methods. Based on the soil arching effect, Chen and Martin (2002) and Liang and Zeng (2002) carried out the numerical simulation analysis on the soil-pile system. In particular, Lee *et al*. (2012) put forward the approach for determining the strongest cantilever beam having a constant volume of the beam material by numerical methods.

There are several methods deal with pile-soil interaction mechanism and the design of the anti-sliding pile; unfortunately, none of them are able to take into account both the characteristics of the landslide and the soil arching effect during studying the load sharing law of the anti-sliding pile. Particularly in the accumulation landslide of the Three Gorges reservoir region, the characteristics of the landslide and the location of the anti-sliding piles are the significant factors to perform the calculation model.

The main purpose of this work is to study the load sharing law of the anti-sliding piles based on the soil arching effect of the Erliban accumulation landslide in the Three Gorges reservoir region. According to a typical case study in the Three Gorges reservoir region, the mechanical interaction model of the Erliban accumulation landslide and anti-sliding piles is developed. Based on the mechanical analysis and numerical modelling using the geotechnical finite difference software FLAC^{3D}, several calculation schemes are presented for comparative analysis and study. This study provides a scientific basis for the standard design of the anti-sliding piles in the Three Gorges reservoir region.

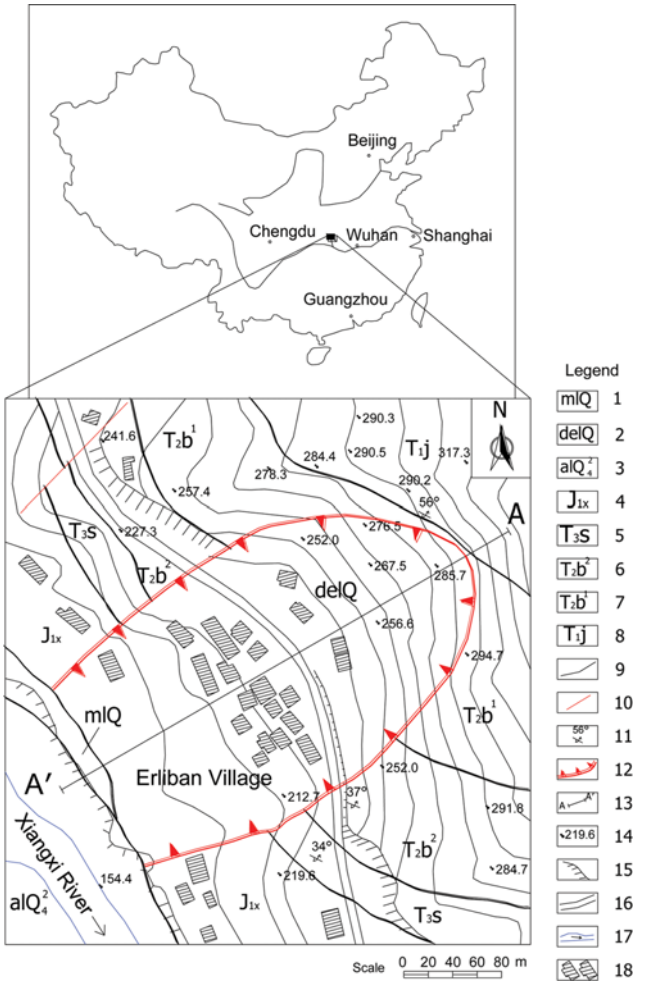

Fig. 1. Sketch Map of Erliban Landslide: (1) Artificial Earth Fill, (2) Eluvium and Deluvium Limestone or Mudstone Gravel with Clay, (3) Alluvium Pebble with Sand, (4) Jurassic Gray Siltstone Intercalated with Silty Mudstone(J_{1x}), (5) Triassic Gray Feldspar Quartz Sandstone Intercalated with Silty Mudstone(T_{3s}), (6) Triassic Purple Red Mudstone (T_{2b}^{2}), (7) Triassic Gray Argillaceous Limestone (T_{2b}^{1}), (8) Triassic Light Gray Limestone(T_{1j}), (9) Geological Boundary, (10) Fault, (11) Attitude, (12) Landslide Mass Boundary, (13) Longitude Profile, (14) Altitude, (15) Cut Slope, (16) Road, (17) River, (18) Houses

2. Geological Condition of the Erliban Landslide

The Erliban landslide is a typical accumulation landslide located on the left bank of the Xiangxi River in Yichang City, China (Fig. 1). Fig. 1 shows that the sliding bed lithology involves five different rock types: Triassic light gray limestone (T_{1j}), Triassic gray argillaceous limestone (T_{2b}^{1}), Triassic purplish red mudstone (T_{2b}^{2}), Triassic gray feldspar Quartz sandstone intercalated with silty mudstone (T_{3s}) and Jurassic gray siltstone intercalated with silty mudstone (J_{1x}). The main sliding trend of the landslide is SW 239°. The width of the landslide at the top is 80 m and at the toe along the river is 180 m. The total volume of the landslide is about 1.45 million m^3, and, hence, it is considered a large-scale landslide. The landslide mass compassed of mainly a mixture of eluvium and deluvium limestone or gravely mudstone with clay (delQ), and the toe of the landslide is composed of artificial earth fill (mlQ). The banks of the river are covered by alluvium, pebbles and sand (alQ_4^2).

3. Theoretical Background

3.1 Soil Arching Effect Test

According to the trap-door test proposed by Chevalier *et al*. (2007), the whole test can be divided into three stages as follows.

Stage I (initial stage): The initial displacement of the mobile door test is quite small (δ is about 1 mm to 3 mm), and the movement is stopped until the vertical load above the mobile door is reduced to the lowest level (Fig. 2(a)). Stage II (transition

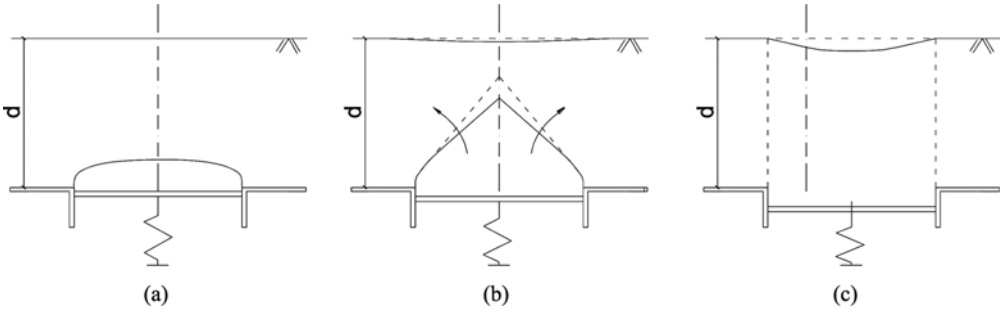

Fig. 2. Illustrate the Three Stages of Chevalier Trap-door Test: (a) Initial Stage, (b) Transition Stage, (c) Final Stage

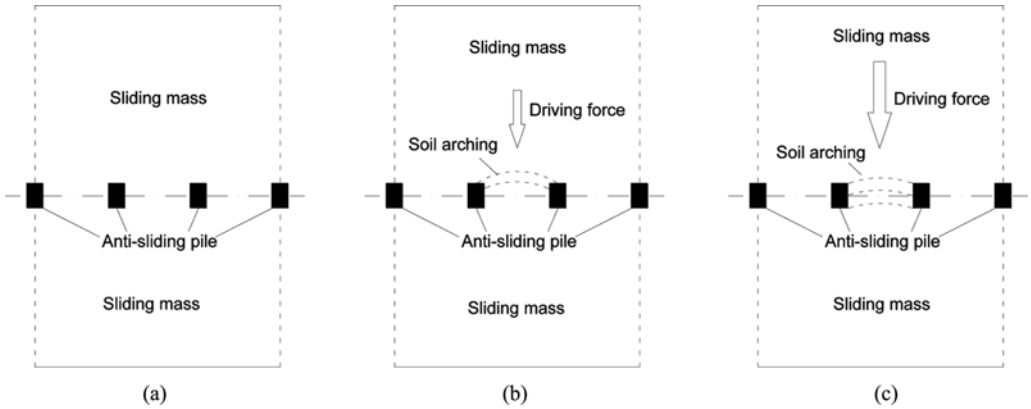

Fig. 3. Illustrate the Three Stages of Interaction Process of the Anti-sliding Pile and Sliding Mass: (a) Initial Stage, (b) Transition Stage, (c) Final Stage

stage): δ is about 3 mm to 40 mm, and the swelled area has spread to the surface of the soil mass to form a wedge shape (Fig. 2(b)). Stage III (final stage): δ *is* about 40 mm to 100 mm, and the two vertical sliding surfaces are shown clearly (Fig. 2(c)).

Based on the three stages of the Chevalier mobile door test, the following conclusions can be stated. (1) The soil arching effect is related to the depth of the soil mass, the width of the mobile door and the engineering properties of the soil mass. (2) The stage characteristics of the soil arching effect are obviously shown during the mobile door test. (3) The soil arching of the 'transition stage' in the second step is the minimum principal stress of soil arching as proposed by Handy (1985). (4) The soil arching of the 'final stage' in the last step is the maximum principal stress of soil arching.

In terms of process, the comparison between the interaction model of the anti-sliding piles and sliding mass and the above mobile door test (Fig. 3) can be analyzed like the mobile door test. The soil arching effect of the soil-pile is related to the depth of the sliding mass, the interval of the piles and the mechanical parameters, especially the strength parameters. The process interaction of the anti-sliding pile and sliding mass can be divided into three stages due to the influence of the thrust force and the pile interval. In addition, the soil arching of the 'transition stage' is the minimum principal stresses of soil arching, while the soil arching of the 'final stage' is the maximum principal stresses of soil arching.

3.2 Theoretical Calculation Model

3.2.1 The Definition of Soil-pile Load Sharing Ratio

The aim of setting the anti-sliding piles is to share the driving force of the landslide mass and to study the load transfer portion of anti-sliding piles. Therefore, the specific ratio of the load transfer portion from the sliding mass to the anti-sliding piles and the total driving force is defined as the pile load sharing ratio. It can be expressed as:

$$\xi = \frac{P_t}{P} \tag{1}$$

Where P_t is the load transfer portion from the sliding mass to the anti-sliding piles (kN/m), and P is the total landslide driving force (kN/m).

3.2.2 The Load Transfer Process

According to the soil arching effect test stated above, the soil arching of the "transition stage" is the minimum principal stress of soil arching, and the soil arching of the "final stage" is the maximum principal stress of soil arching. During the transition stage, soil arching behind the piles plays a dominant role, and part of the landslide's driving force is transferred to the back wall of the piles. During the final stage, soil arching between the piles plays a dominant role, and part of the landslide's driving force is transferred to the sidewall of the piles.

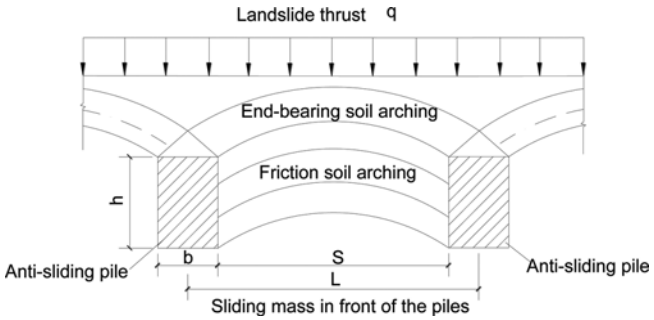

Fig. 4. Three-stages Pile-soil Load Sharing Model

On the basis of the different characteristics of the load transfer process between anti-sliding pile and landslide, the soil arching behind the piles can be called the end-bearing soil arching, and the soil arching between the piles can be called the friction soil arching.

3.2.3 Pile-soil Load Sharing Model

In the traditional soil-pile interaction process, there is no difference between the end-bearing soil arching and the friction soil arching. Therefore, it is difficult to find the actual soil-pile interaction process. In this paper, the three stages pile-soil load sharing model for the anti-sliding pile and landslide interaction is presented as the end-bearing soil arching, friction soil arching and sliding mass in front of the piles (Fig. 4).

Here, (q) is the driving force of the landslide mass (kN/m); *b* and *h* are the width and the height of the anti-sliding pile cross-section (m), respectively; *L* is the interval between the adjacent piles (m); and *S* is the net interval between the adjacent piles (m).

4. Numerical Simulation Computational Model

4.1 Numerical Computation Method

FLAC^{3D} is a three-dimensional explicit finite-difference program for geotechnical engineering computation. It has been widely used in many applications, such as mining engineering, tunnel engineering, and civil engineering. Hakami (2001) carried out the numerical computations to simulate a comprehensive pump test at Sellafield by using FLAC^{3D}. Cai *et al*. (2007) used the FLAC/PFC coupled numerical simulation of acoustic emission in large-scale underground excavations.

4.2 Numerical Modelling

4.2.1 Original Case Model

There are many landslides in the Three Gorges reservoir region, and most of them are accumulation landslides, therefore, an accumulation landslide with anti-sliding piles reinforcement is chosen as the study object.

Based on the analysis of the site investigation data, a comprehensive control scheme involving anti-sliding piles and drainage is presented. In this scheme, the anti-sliding piles are designed to erect the piles at the toe of the landslide to obtain the best control effect (Fig. 5). Fig. 5 presents a typical profile of an accumulation landslide in the Three Gorges reservoir region and the location of the anti-sliding piles, represent the original site to which the numerical modelling will be carried out.

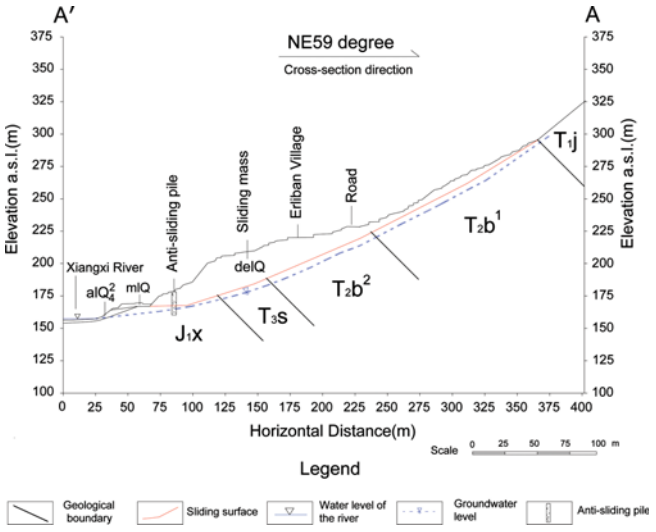

Fig. 5. Cross Section Along A-A' Profile of Erliban landslide

4.2.2 Hypothesis for Calculation Model

In the past twenty years, many scholars simplified the pile-soil interaction model to a planar two-dimensional problem, i.e., a

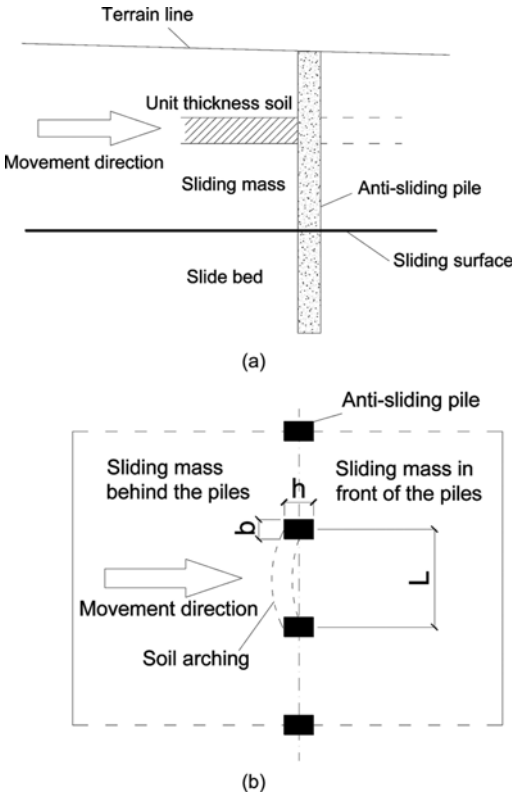

Fig. 6. Simplified Two-dimension Pile-soil Model: (a) Profile Graph, (b) Planar Graph

unit thickness of pile-soil in a certain depth is chosen as the case study (Fig. 6 (a and b)). Based on this model, we hypothesize that: (1) the displacement of the sliding mass is confined to the horizontal direction and (2) the horizontal displacement of the pile is zero.

To determine the proper scale to calculate the model, Chen and Martin (2002) suggested that the boundary space (10*d*, *d* = pile diameter) should be verified by observation of the development of the increase of the soil plasticity as sufficient to represent an isolated pile without inducing group effects.

Instead of the two piles in the traditional calculation model, the four piles were used in the model to avoid the influence of the boundary (Fig. 6). In this model, the intermediate two piles are the key study object.

4.2.3 The Determination of Constitute Model

The soil behaviour is assumed to be an elasto-plastic Mohr-Coulomb material using large strain mode analysis and the coordinates are updated in each step. An isotropic elastic model was used for the anti-sliding pile, and Mohr-Coulomb model was applied to the surrounding soil. In addition, the interface element was used to simulate the friction between the soil mass and the piles.

4.2.4 Constraint Condition for Model

To model the actual slope characteristics of the landslide in the Three Gorges reservoir region, the boundary of the front part of the model should be set free (shown in Fig. 7). The constraint conditions of the anti-sliding piles are restrained in all three dimensions: *X*, *Y* and *Z*.

4.2.5 Geometry Condition for Model

Many authors assume that the cross-section of the pile is circular or square. Actually, the cross-section of the anti-sliding pile is rectangular. Therefore, in this study, the cross height is 1.5 times that of the cross width, i.e., $a = 1.5b$. In order to decrease the influence of the boundary, ten times the height of the pile is left at both parts of the front and back of the pile row (see Fig. 8).

This numerical model of the anti-sliding pile and sliding mass has been validated by the laboratory physical modeling and site investigation, referring to the numerical modelling by Chen and Martin (2002), whose conceptual model has been accepted by many researchers in the field of soil arching; which is referred as the computational model in this paper.

The cross-section width of the anti-sliding pile is equal to 2 m, and the pile height cross-section is 3 m. The interval of *L* is chosen to be four times of the cross-section of width, i.e., $L = 8$ m. Therefore, the numerical model is given in Fig. 8 with a total width and height of 24 m and 63 m, respectively.

4.2.6 Model Parameters

According to the site investigation and laboratory tests of the Erliban landslide, the main parameters involved in the model calculation for the anti-sliding piles and sliding mass soil are shown in Table 1.

With respect to the computational parameters, most of the parameters of the material properties involved in the calculated model are obtained from the laboratory tests, some parameters, such as the normal stiffness and shear stiffness adopted in the paper of Chen and Martin (2002), which are supported by the

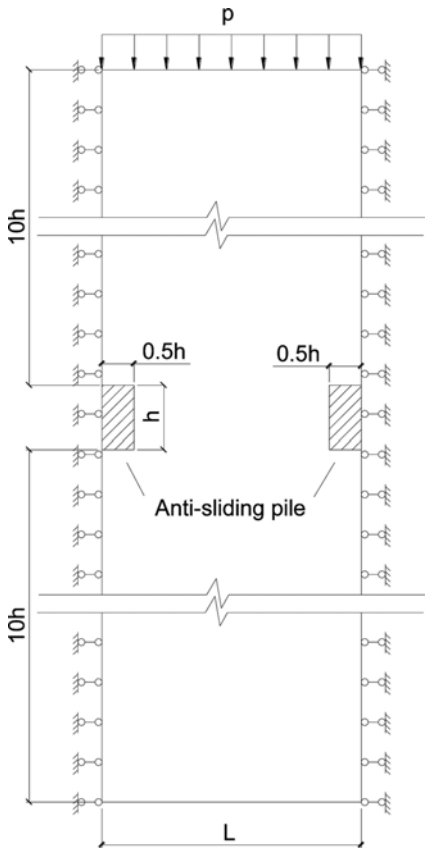

Fig. 7. Improved Constrain Condition for Pile-soil Model

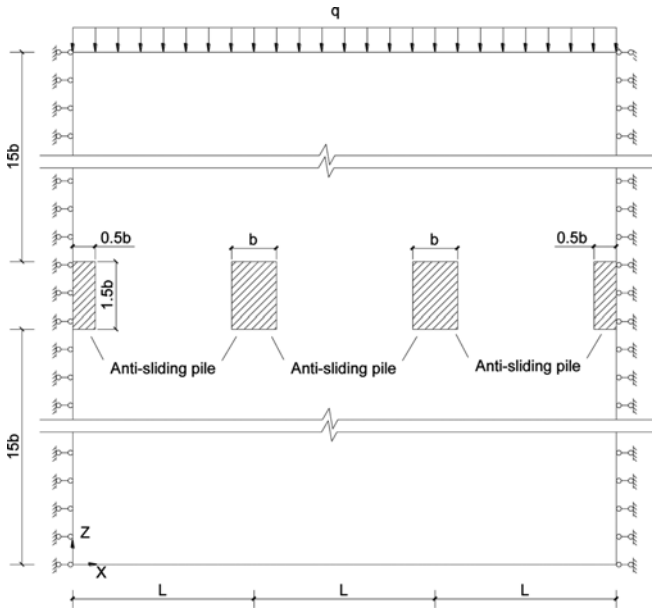

Fig. 8. Numerical Calculation Model for Soil Arching Effect

Table 1. Parameters of the Material Properties Involved in the Calculated Model

Material	Deformation modulus (kPa)	Poisson's ratio	Unit weight (kN/m^3)	Cohesion (kPa)	Internal friction angle (°)
Soil	2.2×10^4	0.3	20.1	45.0	30
Anti-sliding pile	3.0×10^7	0.2	25.5	/	/

plane-strain model for evaluation of arching test. In addition, the initial internal friction of the interface is set to represent the frictional strength of the interface.

To represent the driving force of the sliding mass, a uniform stress q (5.0×10^4 Pa) along the Z direction (see Fig. 8), i.e., the direction of driving force movement, is applied to the upper boundary for the analysis.

4.2.7 Model Meshing

The Y direction in the model presented in this paper is assumed to be the unit thickness. In the case of the XZ plane, the meshing space for the sliding mass is 0.5 m. Therefore, the total number of the meshing nodes is 13594, and the total number of meshing elements is 6501. The interface is set between the sliding mass and the anti-sliding piles (shown in Fig. 9).

The scale of the soil arching effect is located within the blue bold rectangle, as in Fig. 9, because the interval of the piles is 8 m, the number of element zones in the Z direction is 16.

The origin of the coordinates is located in the lower left corner of the graph in Fig. 9. The centre connecting line of the anti-sliding piles, i.e., $z = 31.5$ m, is considered as the basic reference profile. In addition, the front wall and the back walls of the anti-sliding piles are used as standard lines to indicate the distance to the selected profile selected. As for instance, Z profile of the pile-front b indicates the profile whose distance is $b = 2$ m from the front wall of the pile.

5. Three-stage Load Sharing Pattern

Based on the numerical calculation model above, the mechanism of the load transfer in the soil arching effect can be determined by FLAC^{3D} software.

Different representative Z profiles were selected to calculate the normal stress. In the case of the sliding mass in front of the piles, pile-fronts of 0.5b and 2b were selected. The pile-back 0.5b, b and 4b were used to represent the sliding mass in the back side of the piles. The sliding mass between the piles and the centre connecting line are two profiles located at a distance of 0.75b from the central line. The two profiles are called the pile-inter-front 0.75b and pile-inter-back 0.75b, respectively.

To find the different stress distribution in the Z direction under the condition of a free front boundary, eight representative profiles are chosen to show the stress distribution (see Fig. 10). A lot of quantitative data can be obtained from Fig. 11, whose horizontal ordinate is the X direction horizontal distance, and the vertical ordinate is the normal stress. Therefore, the closed area between the stress curve (kPa/m) and the X axis (m) is the total stress (kPa), i.e., the integral of the element stress multiplied by the width of the element. For example, the closed area of the normal stress curve in the Z direction profile ($y = 0$, $x = 0$ and $x = 8$)

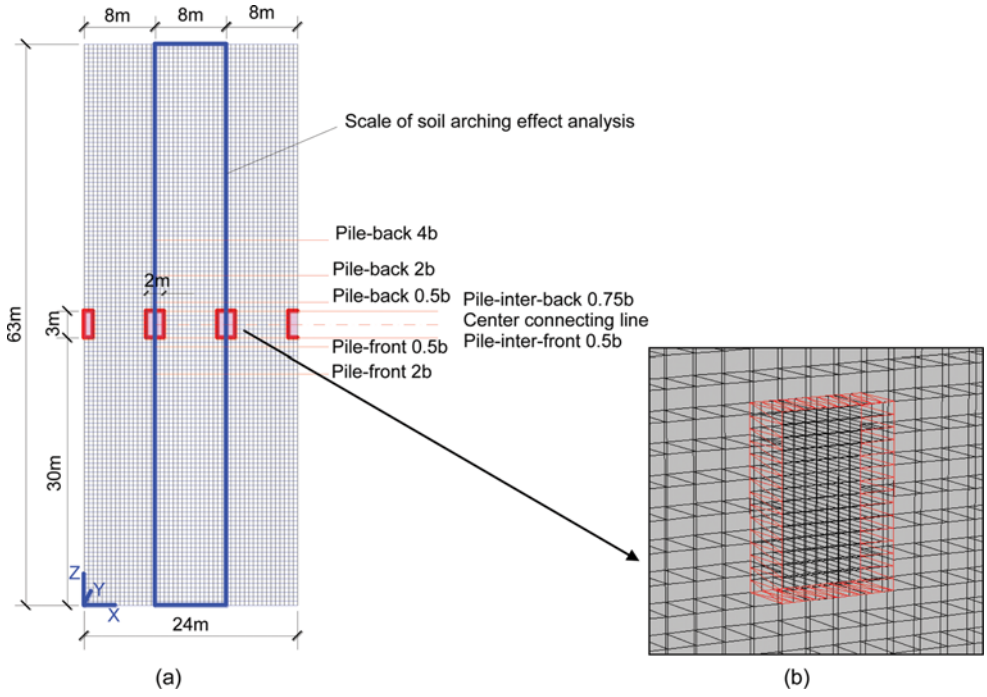

Fig. 9. Meshing Graph for Model with L=4b: (a) Meshing Model, (b) Detailed Interface

is the load applied to the profile. The total load at the upper boundary is the normal stress, 50 kPa, multiplied by the pile interval, 8 m, i.e., 400 kPa.

As indicated in Fig. 10, the normal stress of the pile-back 4*b* profile of *Z* direction is approximately equal to 50 kPa, this means, it is far enough from the back wall of the pile. Therefore, the soil arching effect is very weak beyond the 4*b*, i.e., the effect scale of the soil arching effect is within the 4*b* scale.

Furthermore, the load sharing has changed from pile-back 4*b* to pile-back 0.5*b,* as shown in Fig. 11, the shaded area in Fig. 11 shows the transferring load quantity from the sliding mass to the piles. The transferring load of the profile pile-back b, from the soil mass to the piles is 56.06 kPa. The transferring load of the profile pile-back 0.5*b*, is 94.85 kPa, the latter is much larger than the former. The closer is the distance from the profile to the back wall of the piles, the more is the load transferred from the sliding

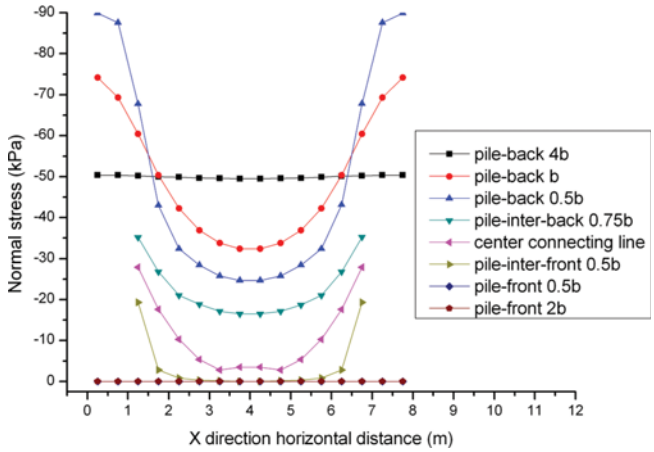

Fig. 10. Stress Distribution of Different *Z* Direction Profiles Along *X* Direction. Note That: The Line of Pile-front 2*b* Is Quite Close to that of the Pile-front 0.5*b*

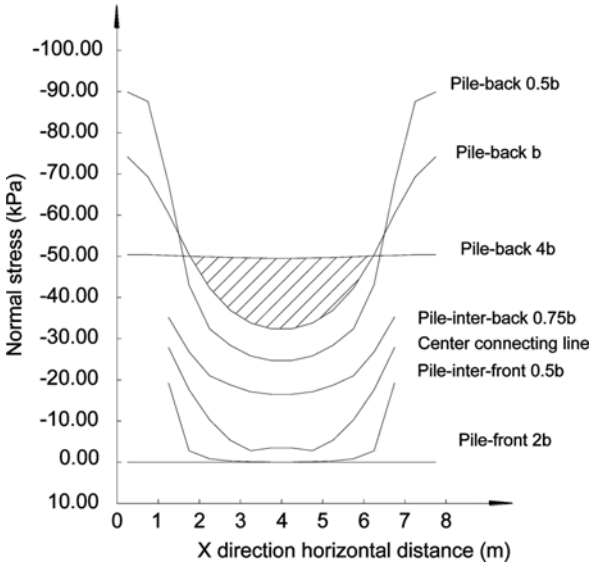

Fig. 11. Load Quantity Transferring from the Sliding Mass to the Piles

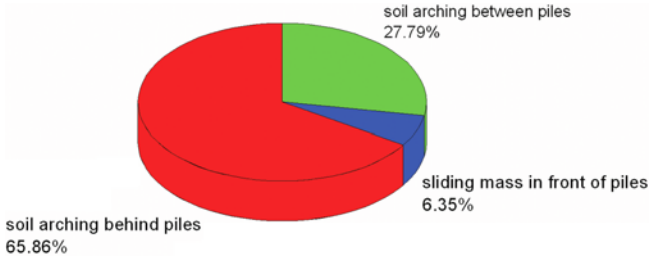

Fig. 12. Comparison Pie Graph of Load Sharing Ratio of Different Soil Arching Along the *Z* Direction

mass to the piles, i.e., the clear is the soil arching effect.

Figure 11 shows that the stressed area of the normal stress curve of the pile-inter-back 0.75*b* profile ($y = 0$, $x = 0$ and $x = 8$) is 136.58 kPa and the stressed area of the normal stress curve of the pile-inter-front 0.75*b* profile ($y = 0$, $x = 0$ and $x = 8$) is 25.42 kPa. Since the total load is 400 kPa, the difference between the total load and the load at the pile-inter-back 0.75*b* is the load undertaken by the soil arching behind the piles, which is 263.42 kPa and represents 65.86% of the total load. For the same reason, the difference between the loads at pile-inter-back 0.75*b* at the pile-inter-front 0.75*b* is the load undertaken by the soil arching between the piles, which is 111.17 kPa and represents 27.79% of the total load. Therefore, there is only 25.41 kPa left for the load transferring to the sliding mass in front of the piles, which is 6.36% of the total load. A pie graph can be drawn in Fig. 12 to show the load sharing percentage for different soil arching. Therefore, we can arrive the conclusion that the load transferring of the pile-soil interaction process is a kind of three-stage load sharing pattern. The soil arching behind the piles and the soil arching between the piles takes most of the total load; therefore, the load percentage for the sliding mass in front of the piles is quite low, and the anti-sliding piles can control the landslide effectively.

6. Different Factors That Influence Soil Arching

6.1 Soil Arching Effect under Different Pile Intervals

In order to study the soil arching effect under different pile intervals, the pile intervals $L = 2b$, $3b$, $4b$, $5b$ and $6b$ are chosen to analyse the relationship between the pile interval and the soil arching effect. In this study, the width of the anti-sliding pile cross section *b* is assumed to be 2 m.

The different pile intervals show different characteristics of the soil arching effect. For $L = 2b$ (Fig. 13), the soil arching between the piles and soil arching behind the piles are shown clearly in Figs. 13(a and b), respectively, and, at the same time, the anti-sliding piles could effectively prevent the deformation spreading from the back part of the piles to the front part of the piles (Fig. 13(c)), when the pile interval $L = 3b$, $4b$, $5b$ and $6b$, the soil arching effect contour graphs can be obtained as indicated by Figs. 14-16 and 17, respectively.

Based on results presented by Figs. 14-16 and 17, the following conclusions can be drawn: (1) As the pile interval increases, the

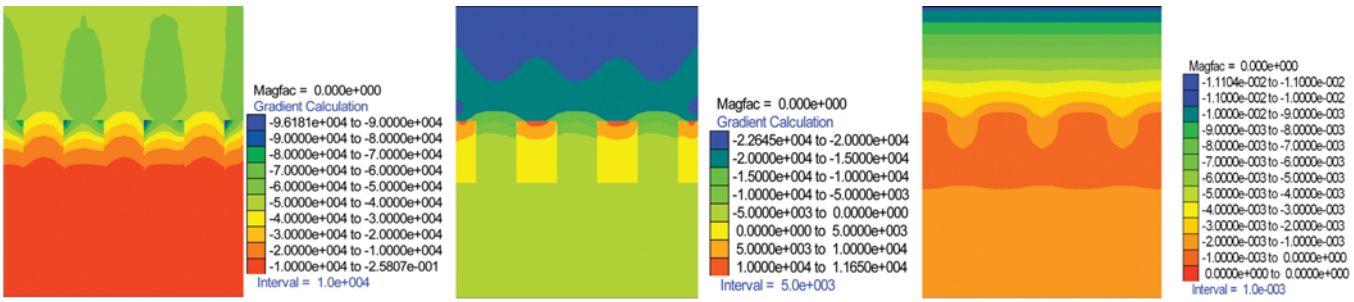

(a) (b) (c)

Fig. 13. Soil Arching Effect Contour Graph under the Case $L = 2b$: (a) Maximum Stress Contour Graph, (b) Minimum Stress Contour Graph, (c) *Z*-direction Displacement Contour Graph

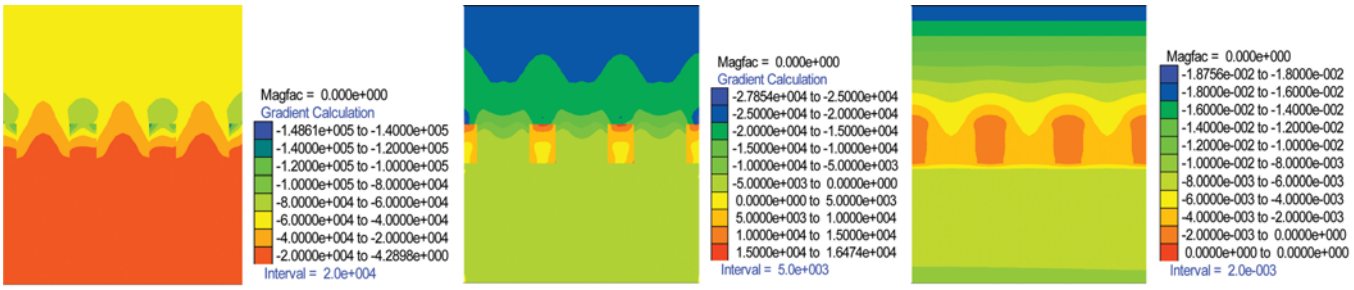

(a) (b) (c)

Fig. 14. Soil Arching Effect Contour Graph under the Case $L = 3b$: (a) Maximum Stress Contour Graph, (b) Minimum Stress Contour Graph, (c) *Z*-direction Displacement Contour Graph

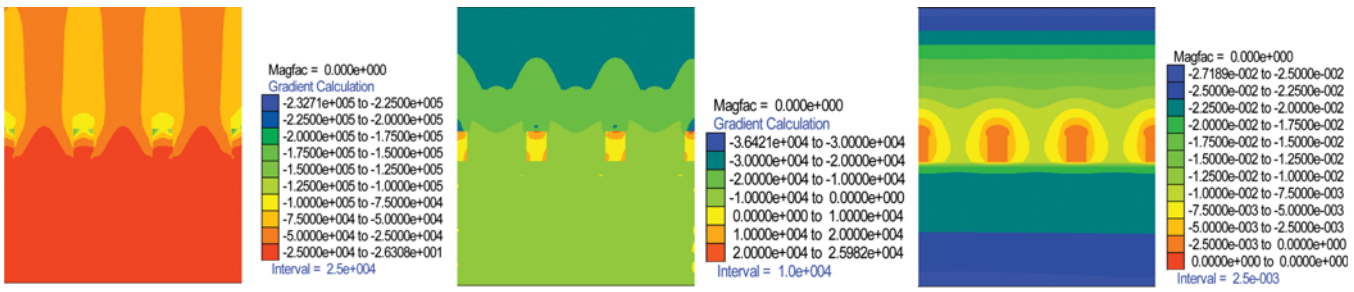

(a) (b) (c)

Fig. 15. Soil Arching Effect Contour Graph under the Case L=4b: (a) Maximum Stress Contour Graph, (b) Minimum Stress Contour Graph, (c) *Z*-direction Displacement Contour graph

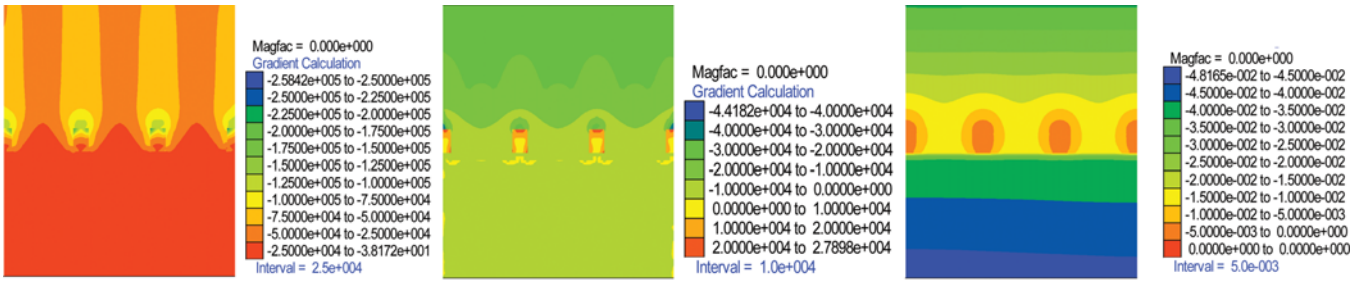

(a) (b) (c)

Fig. 16. Soil Arching Effect Contour Graph under the Case $L = 5b$: (a) Maximum Stress Contour Graph, (b) Minimum Stress Contour Graph, (c) *Z*-direction Displacement Contour Graph

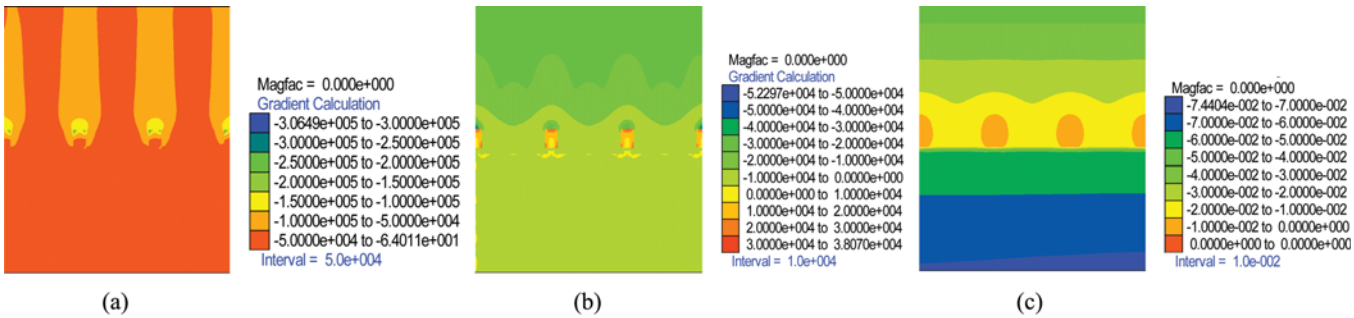

Fig. 17. Soil Arching Effect Contour Graph under the Case $L = 6b$: (a) Maximum Stress Contour Graph, (b) Minimum Stress Contour Graph, (c) Z-direction Displacement Contour Graph

effect of soil arching behind the piles becomes weaker until it disappears, but the effect of soil arching between the piles becomes stronger until the pile interval reaches a certain limit value. (2) From the maximum stress contour graph, the maximum stress of the soil arching acted on the sidewall of the adjacent piles is formed as a result of the soil mass between the piles. The stress skewback the soil arching is on the sidewall of the piles. As the pile interval L increases, the thickness of the soil arching became thinner. When the pile interval is larger than 5b, the soil arching effect almost disappears. (3) According to the minimum stress contour graph, the minimum stress soil arching acted on the back wall of the adjacent piles is caused by soil mass behind the piles. The stress skewback the soil arching between the piles is in the back wall of the piles. As the pile interval L increases, the soil arching becomes weaker. When the pile interval is larger than 5b, the soil arching effect behind the piles almost disappears. (4) From the Z direction of the displacement contour graph, the displacement of the anti-sliding piles is almost equal to zero because of its huge stiffness. On the contrary, the displacement of the sliding mass increases with the increase of the pile interval.

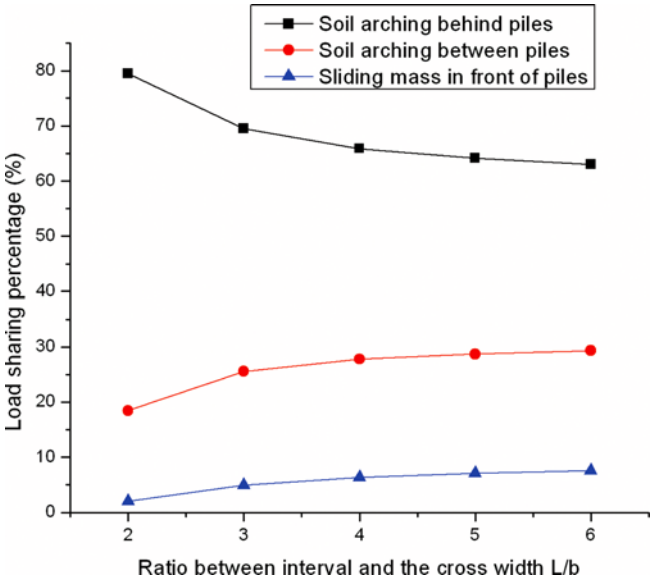

Fig. 18. Different Grade of Loads Transferring Graphs under Different L/b

6.2 Pile Nterval Influence on the Load Sharing Ratio

The pile interval not only affects the soil arching effect but also it has an influence on the load sharing ratio process. To better explain the analysis, the ratio between the pile interval and the cross section width (L/b) is defined to describe the relationship between the pile interval and the pile cross section.

The width of the pile section b is set to 2 m. The pile intervals are $L = 2b$, 3b, 4b, 5b and 6b. The analysis process is similar to that above. The different grades of the load transferring graphs under different L/b are shown in Fig. 18.

The results obtained from Fig. 18 show that the load undertaking proportion of the soil arching behind the piles drops gradually to some extent until it reaches a stable value, which is the exact load that directly acts on the back wall of the piles. With respect to the soil arching between the piles and the sliding mass in front of the piles, their load undertaking proportion rises gradually to some extent until it reaches a stable value.

6.3 Analysis on Differential Displacement in Soil Arching

The soil arching effect is caused by the differential displacement, basically, influences the pile load sharing ratio.

As indicated in Figs. 13-17, different pile intervals have different impact on the Z-direction displacement contour graph. Under the cases $L = 2b$ and $L = 3b$, the displacement contour graph between the anti-sliding piles is integral, which shows that the soil arching is stable under these cases. On the contrary, the displacement contour graph between the anti-sliding piles is divided by the driving force under the cases $L = 4b$, $L = 5b$, and $L = 6b$, which means that the soil arching has been broken. Therefore, we can arrive to the conclusion that the soil arching only exits within a certain pile interval, and it will become inefficient beyond the maximum pile interval. These analysis results can be also validated by the minimum and maximum stress contour graph.

6.4 Influence of the Sliding Mass Parameters on the Load Sharing Ratio

6.4.1 Influence of Sliding Mass Cohesions on Load Sharing Ratio

When the internal friction angle equal to 30°, different cohesion

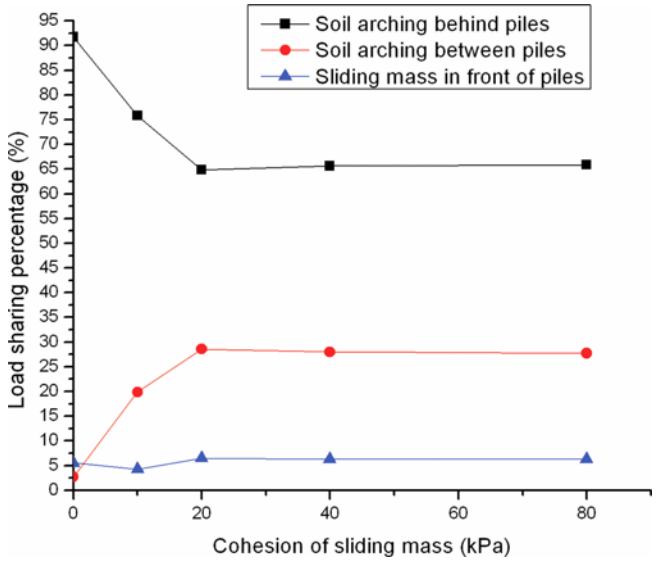

Fig. 19. Different Grade Loads Transferring Graphs under Different Cohesion Values

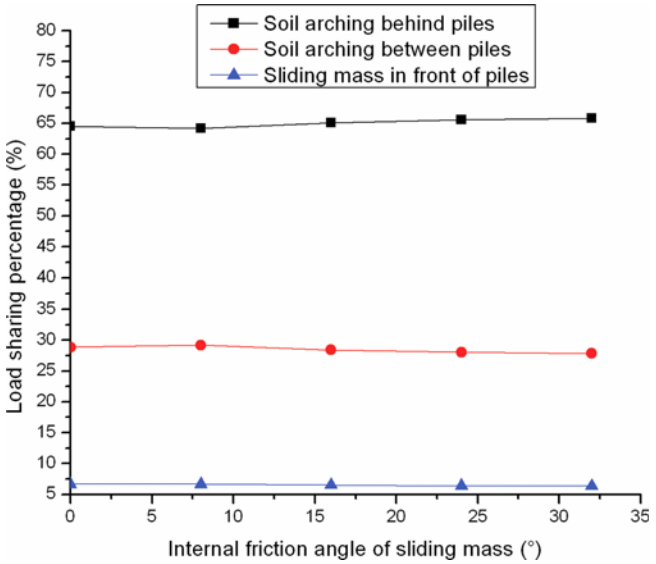

Fig. 20. Different Grade Loads Transferring Graphs under Different Internal Friction Angles

(c) values (0 kPa, 10 kPa, 20 kPa, 40 kPa, 80 kPa) are chosen to study the load transferring law under the condition L=2b. The different grade load transferring graphs under the different cohesive parameters are shown in Fig. 19.

According to Fig. 19, the load undertaken by the soil arching behind the piles drops down quickly to some extent until it reaches a stable value with the increase of cohesion of the sliding mass. On the other hand, the load undertaken by the soil arching between the piles rises rapidly to some extent until it reaches a stable value. The change in the threshold value of the cohesion from the unstable to stable state is about 20 kPa, which means that the increase of the cohesiveness of the sliding mass will enhance the effect of the soil arching until it reaches 20 kPa.

6.4.2 Influence of Internal Friction Angles of the Sliding Mass on Load Sharing Ratio

The cohesion of the sliding mass was set to 30 kPa, and different internal friction angles ϕ (0°, 8°, 16°, 24°, 32°, respectively) are chosen to study the load transferring law under the condition $L = 2b$. The different grade load transferring graphs under different internal friction angles are represented by Fig. 20.

Fig. 20 shows that the load undertaken by the soil arching in the three stages is almost constant with the increase of the internal friction angle of the sliding mass. The results reveal that the internal friction angle of the sliding mass has limited influence on the effect of soil arching.

6.5 Influence of the Pile-soil Interface on the Load Sharing Ratio

Chen and Martin (2002) conducted soil-pile numerical modelling to simulate the roughness of the interface between the soil and pile by the friction angle parameters of the interface using FLAC. Under the condition that, the other parameters above are the stable, different internal friction angles (0°, 10°, 15°, 25°, 35°)

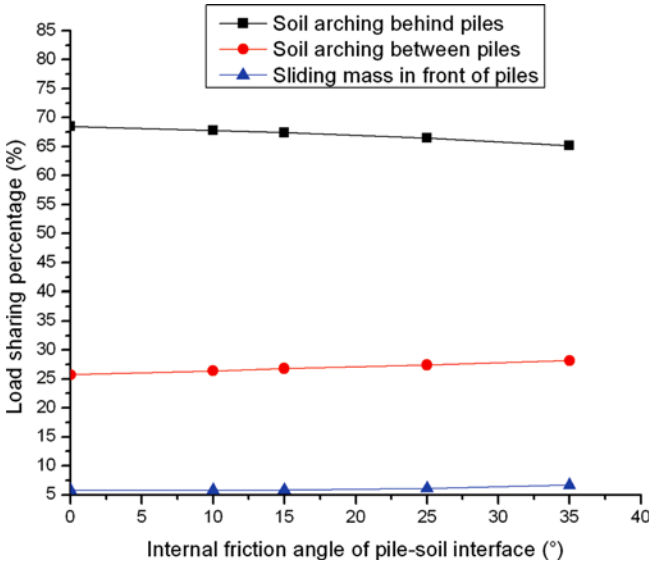

Fig. 21. Different Grade Loads Transferring Graphs under Different Friction Parameters of Interface

of the interface were chosen to carry out the study. Fig. 21 shows the different grade load transferring graphs under different internal friction angles of the interface. The results show that the load undertaken by the soil arching behind the piles decreases slightly when the internal friction angle of the interface increases, while the load undertaken by the soil arching between the piles increases gradually. In general, the internal friction angle of the interface has a slight influence on the effect of the soil arching.

6.6 Influence of the Driving Force on the Load Sharing Ratio

Assuming that the other parameters above were the same, the different driving force (10 kPa, 20 kPa, 40 kPa, 80 kPa, and 120 kPa) are selected to carry out the study on load transferring

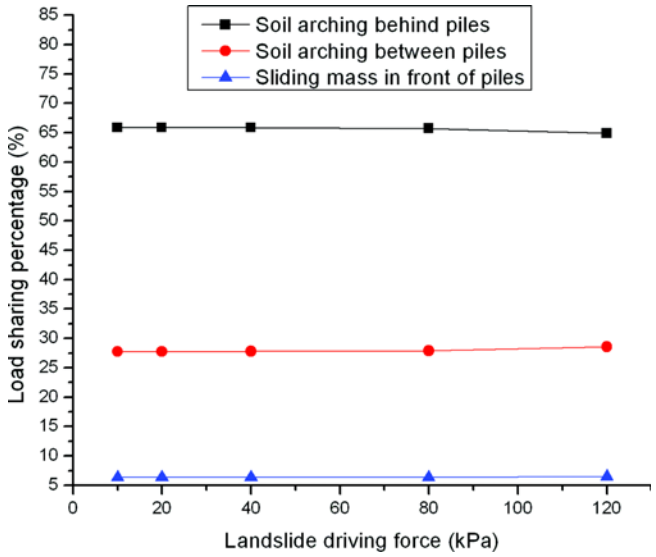

Fig. 22. Different Grade Loads Transferring Graphs under Different Landslide Driving Force

law. The different grade load transferring graphs for different internal friction angles of the interface are shown in Fig. 22. The load undertaken by the soil arching behind the piles decrease slightly with the increase of the driving force loads, while the load undertaken by the soil arching between the piles increase slightly.

The results show that the above factors play significant roles in the effect of the soil arching between the anti-sliding piles and sliding mass. In general, the pile interval and the driving force are two key factors, and increasing the pile interval or driving force weakens the soil arching effect markedly. Due to the close relationship between the pile interval and the soil arching, we can by means of soil arching effect analysis to determine the pile interval computational model in the further study.

7. Conclusions

The process of anti-slide pile and landslide interaction is similar to Terzaghi's trap door test, it can be divided into three stages: initial stage, transition stage and final stage. This model is defined to describe the extent of load transfer from the sliding mass to the anti-slide pile, and it can weigh the effectiveness of anti-sliding. A new model of the load sharing law with a three-stage load sharing pattern was proposed via a representative case study in the Three Gorges reservoir region, China. The law of the load sharing ratio for different cases, including different intervals, cross-section dimensions, driving forces, and shearing parameters of the sliding mass and pile-soil interface, has been examined in detail using the explicit finite-difference numerical modelling method. The results show that these factors play significant roles in the effect of the soil arching between the anti-sliding piles and sliding mass. The effect scale of the soil arching effect is within the scale of four times of the width of the pile. In general, the pile interval and the driving force are two key factors, and increasing the pile interval or driving force weakens the soil arching effect markedly. The soil arching only exits within a certain pile interval, and it will become inefficiency beyond the maximum pile interval. With respect to the strengthened parameters of the sliding mass, when the cohesion or the internal friction angle increases to a certain threshold value, the load sharing ratio between the soil arching behind the piles and the soil arching between the piles remains in a steady level. There is little effect on the soil arching when the strengthened parameters of the sliding mass continue to increase beyond the threshold value.

To design an anti-sliding pile, the roughness of the interface between the pile and the soil should be enhanced. The determination of the pile interval should be related to the driving force of the landslide: The larger is the driving force, the closer is the pile interval, and vice versa. Due to the close relationship between the pile interval and the soil arching, we can by means of soil arching effect analysis to determine the pile interval computational model in the further study. This study provides a new concept and a scientific method to guide anti-sliding pile design for landslide control projects in the Three Gorges reservoir region.

Acknowledgements

The work was funded by National Natural Science Foundation of China (No. 41202198 and 41230637), National Basic Research Program of China (973 Program) (No.2011CB710604), the Special Fund for Basic Scientific Research of Central Colleges, China University of Geosciences (Wuhan) (CUG130409 and CUG090104). The authors would like to extend their most sincere gratitude to the Editors and Reviewers who provided help during the writing of this paper. In particular, the author would like to express the most sincere appreciation to Dr. Mutasim Adam for his help during this study.

References

Cai, M., Kaiser. P. K., and Morioka H. (2007). "FLAC/PFC coupled numerical simulation of AE in large-scale underground excavations." *International Journal of Rock Mechanics and Mining Sciences*, Vol. 44, No. 4, pp. 550-564.

Chen, C. Y. and Martin, G. R. (2002). "Soil-structure interaction for landslide stabilizing piles." *Computers and Geotechnics*, Vol. 29, No. 5, pp. 363-386.

Chevalier, B., Combe, G., and Villard P. (2007). *Load transfers and arching effects in granular soil layer,* 18eme Congres Franrais de Mecanique, Grenoble, France, pp. 27-31.

De Beer, E. E. and Wallays, M. (1972). "Forces induced in piles by unsymmetrical surcharge on the soil around the piles." *Proc. 5th Int. Conf. Soil Mech.*, Madrid, Spain, Vol. 1, pp. 325-332.

Fan, C. C. and Long, J. H. (2005). "Assessment of existing methods for predicting soil response of laterally loaded piles in sand." *Computers and Geotechnics*, Vol. 32, No. 4, pp. 274-289.

Franx, C. and Boonstra, G. C. (1948). "Horizontal pressures on pile foundation." *Proc. 2th Int. Conf. on soil mech and Found. Eng.*

Rotterdam, The Netherlands, Vol. 1, pp. 131-135.
Hakami, H. (2001). "Rock Characterisation Facility (RCF) shaft sinking - Numerical computations using FLAC." *International Journal of Rock Mechanics and Mining Sciences*, Vol. 38, No. 1, pp. 59-65.
Handy, R. L. (1985). "The arch in soil arching." *Journal of Geotechnical Engineering*, Vol. 111, No. 3, pp. 302-318.
Heyman, L. (1965). "Measurement of the influence of lateral earth pressure on pile foundations." *Proc. of 6 th Int. Conf. on Soil Mech and Found. Eng*., Paris, Vol. 2, pp. 257-260.
Ito, T. and Matsui, T. (1975). "Methods to estimate lateral force acting on stabilizing piles." *Soils and Foundations*, Vol. 15, No. 4, pp. 43-59.
Jeong, S., Kim, B., Won, J., and Lee, J. (2003). "Uncoupled analysis of stabilizing piles in weathered slopes." *Computers and Geotechnics*, Vol. 30, No. 8, pp. 671-682.
Jiang, J. C. and Yamagami, T. (2006). "Charts for estimating strength parameters from slips in homogeneous slopes." *Computers and Geotechnics*, Vol. 33, Nos. 6-7, pp. 294-304.
Jiang, J. C. and Yamagami, T. (2008). "A new back analysis of strength parameters from single slips." *Computers and Geotechnics*, Vol. 35, No. 2, pp. 286-291.
Lee, B. K., Lee, T. E., and Jung, Y. S. (2012). "Numerical Methods for Determining Strongest Cantilever Beam with Constant Volume." *KSCE Journal of Civil Engineering*, KSCE, Vol. 16, No. 1, pp.169-178.
Leussink, H. and Wenz, K. P. (1969). "Storage yard foundations on soft cohesive soils." *Proc. of 7th Int. Conf. on Soil Mech and Found. Eng*., Moscow, Russia, pp. 149-155.
Li, C. D., Tang, H. M., Hu, X. L., Wang, L. Q., and Hu, B. (2010). "A new evaluation model for spatial slope prediction based on scale effect law." *The 11th IAEG Congress*, Geological Active, Auckland, New Zealand, pp. 3213-3221.
Liang, R. and Zeng, S. (2002). "Numerical study of soil arching mechanism in drilled shafts for slope stabilition." *Soils and Foundations*, Vol. 42, No. 2, pp. 83-92.
Martin, G. R. and Chen, C. Y. (2005). "Response of piles due to lateral slope movement." *Computers and Structures*, Vol. 83, Nos. 8-9, pp. 588-598.
Matsui, T., Hong, W.P., and Ito, T. (1982). "Earth pressure on piles in a row due to lateral soil movements." *Soils and Foundations*, Vol. 22, No. 2, pp. 71-81.
Poulos, H. G. (1973). "Analysis of piles in soil undergoing lateral movement." *J. Soil. Mech. Found Div.,* ASCE, Vol. 99, No. SM5, pp. 391-406.
Shen, Z. J. (1992). "The slide-resistant force of pile and the limit design for anti-sliding piles." *Chinese Journal of Geotechnical Engineering*, Vol. 14, No. 1, pp. 51-56.
Terzaghi, K. (1943). *Theoretical soil mechanics,* John Wiley & Sons, New York, pp. 76-85.
Uzuokaa, R., Cubrinovskib, M., and Sugitac, H. (2007). "Prediction of pile response to lateral spreading by 3-D soil-water coupled dynamic analysis: Shaking in the direction perpendicular to ground flow." *Soil Dynamics and Earthquake Engineering*, Vol. 28, No. 6, pp. 436-452.
Vardoulakis, L., Graf, B., and Gudehus, G. (1981). "Trap-door problem with dry sand: A statical approach based upon model test kinematics." *International Journal for Numerical and Analytical Methods in Geomechanics*, Vol. 5, No. 1, pp.57-78.
Wang, F. W. and Sassa, K. (2002). "A modified geotechnical simulation model for the areal prediction of landslide motion." *Proc. of 1st European Conf. on Landslides*, Prague, Czech Republic, pp. 735-740.
Wang, G. H. and Sassa, K. (2003). "Pore-pressure generation and movement of rainfall-induced landslides: Effects of grain size and fine-particle content." *Engineering Geology*, Vol. 69, Nos. 1-2, pp. 109-125.
Wang, F. W. and Sassa, K. (2010). "Landslide simulation by a geotechnical model combined with a model for apparent friction change." *Physics and Chemistry of the Earth*, Vol. 35, Nos. 3-5, pp. 149-161.
Wang, G. H., Sassa, K., and Fukuoka, H. (2003). "Downslope volume enlargement of a debris slide-debris flow in the 1999 Hiroshima, Japan, rainstorm." *Engineering Geology*, Vol. 69, Nos. 3-4, pp. 309-330.
Wei, W. B. and Cheng, Y. M. (2009). "Strength reduction analysis for slope reinforced with one row of piles." *Computers and Geotechnics*, Vol. 36, No. 7, pp. 1176-1185.
Wei, W. B., Cheng, Y. M., and Li, L. (2009). "Three-dimensional slope failure analysis by the strength reduction and limit equilibrium methods." *Computers and Geotechnics*, Vol. 36, No. 1, pp. 70-80.
Wenz, K. P. (1973). "Large scale tests for determination of lateral loads on piles in soft cohesive soils." *Proc. of 8th Int. Conf. on Soil Mech and Found. Eng.*, Moscow, Russia, pp. 110-116.
Won, J., You, K., Jeong, S., and Kim, S. (2005). "Coupled effects in stability analysis of pile-slope systems." *Computers and Geotechnics*, Vol. 32, No. 4. pp. 304-315.